Chapter 12 Applications of Remote Sensing

12.1 Land Cover Classification

Land cover mapping is one of the most important and typical applications of remote sensing data. Land cover corresponds to the physical condition of the ground surface, for example, forest, grassland, concrete pavement etc., while land use reflects human activities such as the use of the land, for example, industrial zones, residential zones, agricultural fields etc.

Generally land cover does not coincide with land use. A land use class is composed of several land covers. Remote sensing data can provide land cover information rather than land use information.

Initially the land cover classification system should be established, which is usually defined as levels and classes. The level and class should be designed in consideration of the purpose of use (national, regional or local), the spatial and spectral resolution of the remote sensing data, user's request and so on.

The definition should be made as quantitatively clear as possible. Table 12.1.1 shows an example of land cover classes for land cover mapping in the Sagami River Basin, Japan, for use with Landsat MSS data.

The classification was carried out as follows.

a. Geometric correction (see 9.4)
A geo-coded Landsat image was produced.

b. Collection of the ground truth data (see 6.7)
A ground investigation was made to identify each land cover class on the geo-code Landsat image as well as on topographic maps.

c. Classification by Maximum Likelihood Method (see 11.5)
The Maximum Likelihood Method was adopted using the training samples obtained from the ground truth.

Figure 12.1.1 shows the original image in the Sagami River Basin, while Figure 12.1.2 shows the classified land cover map.

Generally Landsat MSS imagery can provide about about ten land cover classes, depending upon the size and complexity of the classes.

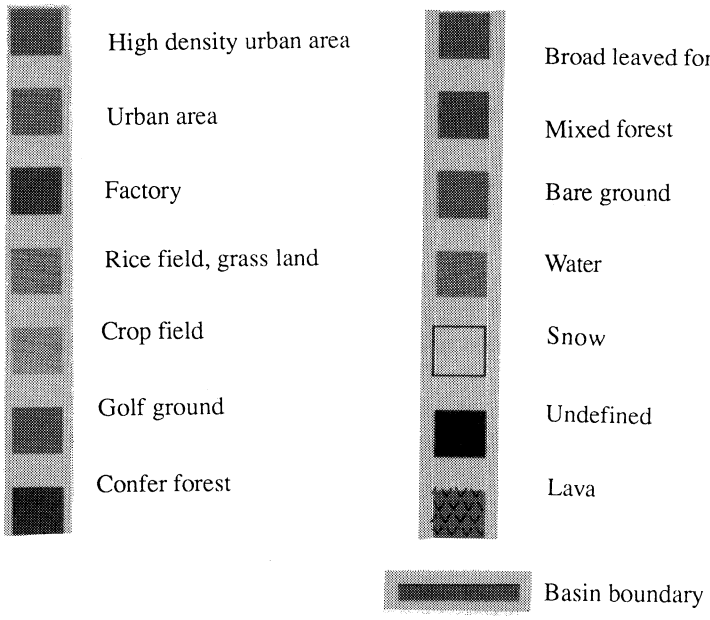

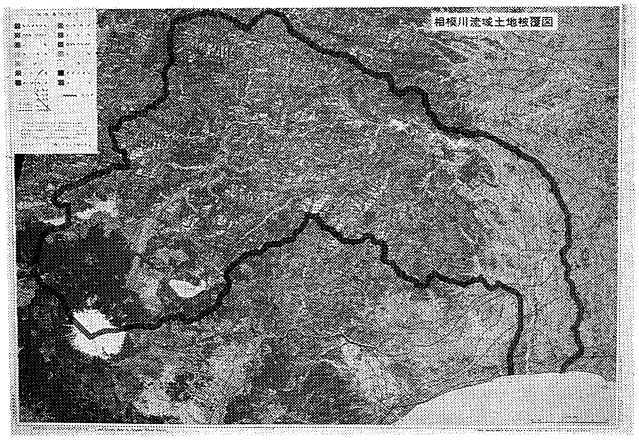

Figure 12.1.1 Land cover classification by Landsat MSS data

(see frontispiece 1)

12.2 Land Cover Change Detection

Land cover change detection is necessary for updating land cover maps and the management of natural resources. The change is usually detected by comparison between two multi-date images, or sometimes between an old map and an updated remote sensing image.

The method of change detection is divided into two;

a. comparison between two land cover maps which are independently produced
b.change enhancement by integrating two images into a color composite or principal component image.

Figure 12.2.1 shows the changes over a 5 year period, which were detected by using a color composite with blue assigned to an old image of Landsat TM and red assigned to a new image of Landsat TM.

Such detection is very useful for updating "vegetation maps" of 1:50,000 to 1:100,000 scale with Landsat TM or SPOT, and of 1:250,000 scale with Landsat MSS.

The land cover change can also be divided into two;

a. **seasonal change**
agricultural lands and deciduous forests change seasonally

b. **annual change**
land cover or land use changes, which are real changes, for example deforested areas or newly built towns.

Usually seasonal change and annual change are mixed within the same image. However only the real change should be detected, so that two multi-data images of almost same season should be selected to eliminate the effects of seasonal change. One should note that a cycle of seasonal change can be rather complex as shown in Figure 12.2.2. Sometimes seasonal change rate is very high, for example in spring time in cold area.

Figure 12.2.1 Land cover change area on a vegetation map

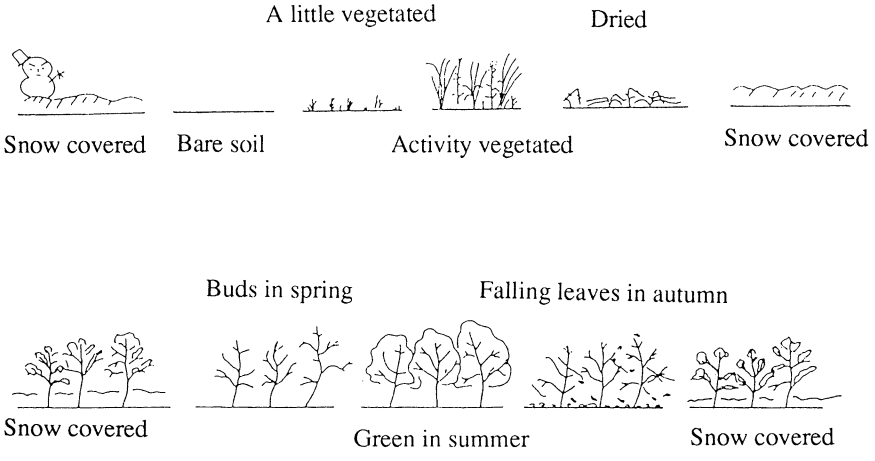

Figure 12.2.2 Seasonal change of grassland (upper) and deciduous (lower)

12.3 Global Vegetation Map

NOAA **AVHRR** data (see 5.1) are very useful for producing a global vegetation maps which cover the whole world, because NOAA has edited global cloud free mosaics in the form of a **GVI**(global vegetation index) on a weekly basis since April of 1982.

The GVI data include information about **NDVI** (normalized difference vegetation index) as computed as follows

$$NDVI = \frac{Ch.2-Ch.1}{Ch.2+Ch.1}$$

Ch.1 : visible band
Ch.2 : near infrared band

NDVI is sometimes simply called. NVI (normalized vegetation index).

NDVI or NVI are indicators of the intensity of biomass.

The larger the NVI is, the denser the vegetation.

Though the original resolution of NOAA AVHRR is 1.1 km per pixel of the Equator, the GVI has a low resolution of 16 km x 16 km per pixel at the Equator. In spite of the low resolution, the GVI is useful for producing a global vegetation map.

As much noise is involved in weekly data, noise free GVI compiled on a monthly base should be used. Figure 12.3.1 shows six categories out of a total of 13 categories obtained from cluster analysis (see 11.2).

Figure 12.3.2 shows the result of a cluster analysis applied to GVI data from 1987.

Though the clustered map in Figure 12.3.2 has not yet been verified, it shows the possibility of using remote sensing data for global map production.

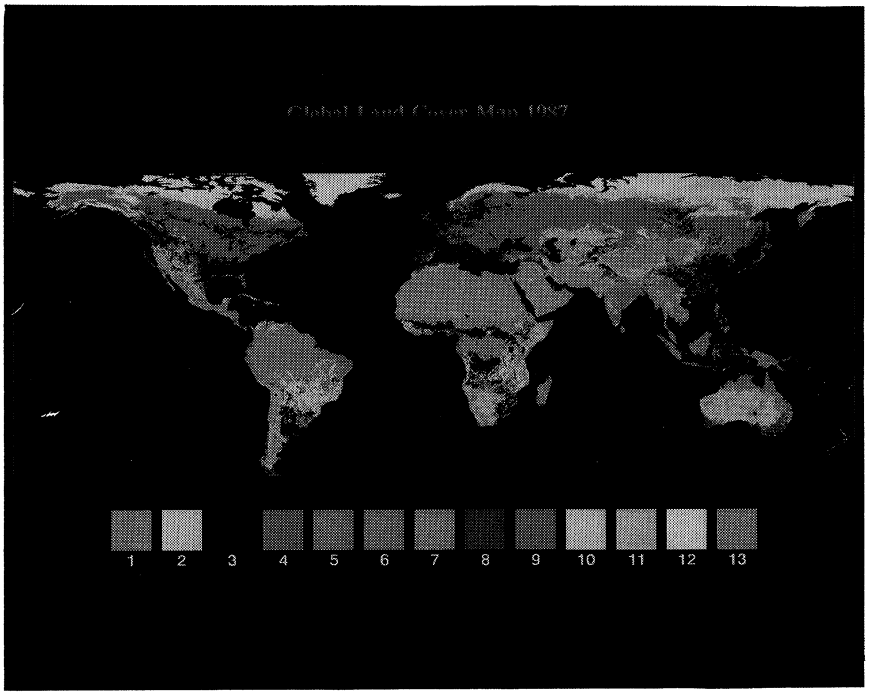

Figure 12.3.1 Global vegetation map by NOAA NDVI data
(see frontispiece 4)

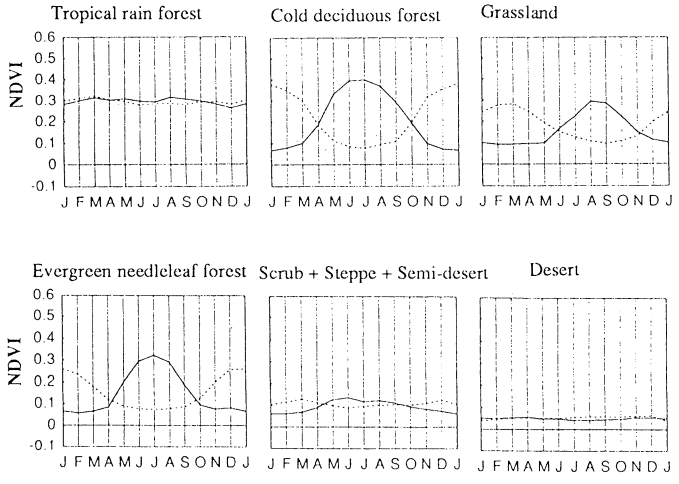

Figure 12.3.2 Vegetation seasonal dynamics of each category in figure 12.3.1

12.4 Water Quality Monitoring

Water pollution has become a very serious problem in big cities and in offshore areas along industrial zones. Water quality monitoring is one of the typical applications of remote sensing.

Figure 12.4.1 shows the characteristics of reflection, absorption and scattering on the water surface, beneath the surface water and from the bottom. The sea color depends on the absorption and scattering due to water molecules and suspended particles or plankton.

Figure 12.4.2 shows various curves of spectral attenuation with respect to various types of water. As seen in the figure, clear water has a peak of minimum attenuation around 0.5 μm, while turbid water with **suspended solid (SS)** has larger attenuation with a minimum peak around 0.55 μm. In other word, radiation can penetrate into deep clear water and is scattered by the water volume, causing the typical bluish color. Turbid waters cannot be penetrated and radiation is scattered near the surface, giving a greenish or yellowish color.

The sea color depends on not only on suspended solids but also the **chlorophyll** of plankton within the water body.

Figure 12.4.3 shows an example of the measurement for spectral reflectance of various amounts of chlorophyll. As seen in the figure, chlorophyll in the sea can be detected in the region of 0.45 - 0.65 μm.

Figure 12.4.4 shows the distribution of chlorophyll around the Indian Sea derived from CZCS (coastal zone color scanner) data of Nimbus 7.

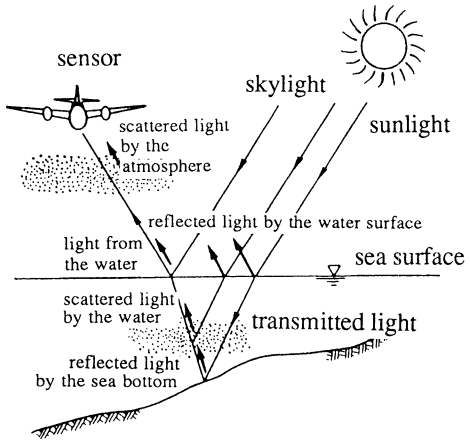

Figure 12.4.1 Incident light into a sensor on the sea

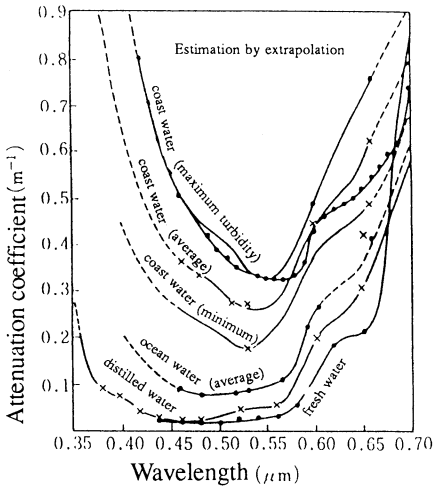

Figure 12.4.2 Spectral attenuation characteristics of water

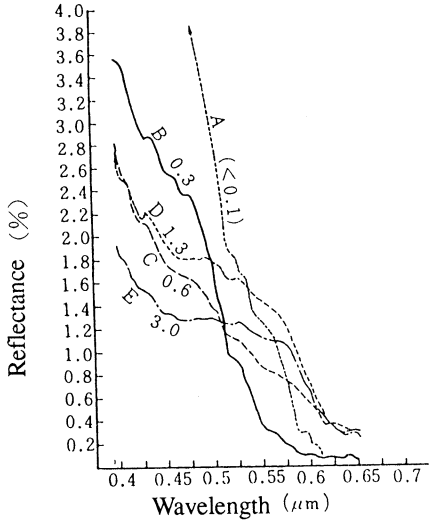

Figure 12.4.3 Spectral reflectance of water with chlorophyll

12.5 Measurement of Sea Surface Temperature

Satellite remote sensing can provide thermal information in a short time over a wide area. Temperature measurement by remote sensing is based on the principle that any object emits electro-magnetic energy corresponding to the temperature, wavelength and emissivity.

The temperature detected by a thermal sensor is called the "**brightness temperature**" (see 1.7). Though the brightness temperature coincides with the real temperature if the objects is a black body, the actual object on the earth has a different **emissivity** e ($e < 1$) which emits electro-magnetic energy of e.I, where I indicates the radiance of a black body with the same temperature.

Thus the value of e as well as the emitted radiance should be measured in order to compute the exact temperature, as explained in Figure 12.5.1.

However the value of e for sea water is very nearly equal to 1 and also comparatively constant, while the value e for ground surfaces is not homogeneous. Thus sea surface temperature can be estimated more accurately than ground surface temperature.

As the actual brightness temperature includes emitted radiance from the atmosphere, this will cause a temperature error ranging 2-3 degrees Centigrade between the actual sea surface temperature and calculated brightness temperature from satellite data. Thus atmospheric correction (see 9.2) is very important for accurate sea surface temperature measurement.

Figure 12.5.2 shows the sea surface temperature in pseudo color in Northern Japan using NOAA AVHRR data which were atmospheric ally as well as geometrically corrected with overlays of sea coast lines and latitude and longitude grid lines.

Using the most recent technology, the estimated accuracy of sea surface temperature is claimed to be about ±0.5℃ on a global scale and about ±0.3℃ on a regional scale.

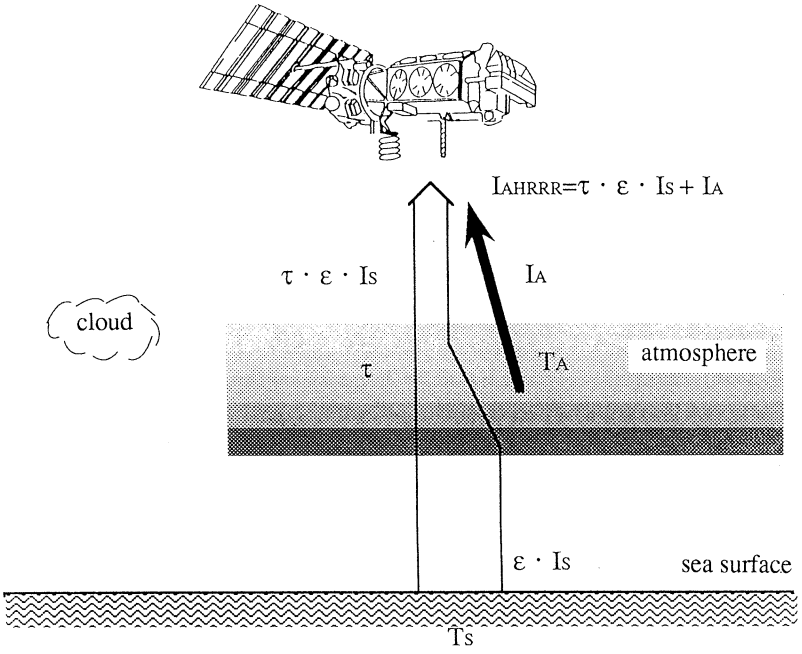

TS	: sea surface temperature
IS	: electromagnetic energy emitted form black body at temperature TS
ε	: emissivity of atmosphere
τ	: transmittance of atmosphere
TA	: average temperature of atmosphere
IA	: electromagnetic energy emitted form atmosphere at temperature TA
IAVHRR	: electromagnetic energy detected by AVHRR sensor

Figure 12.5.1 Sea surface temperature measurement

12.6 Snow Survey

As snow cover has a very high reflectance, the aerial distribution of snow can be identified very easily from satellite remote sensing data. Several models to estimate water resources in units of **snow water equivalent** have been proposed with use of the estimated snow cover area.

Figure 12.6.1 shows a conceptual diagram of the estimation of basin-wide snow water equivalent with the three parameters of elevation h, latitudinal distribution of snow water equivalent S(h) and hydrometric curve A(h).

Snow water equivalent Ss in a river basin can be computed as follows.

$$S_S = \int_{h_L}^{h_H} S(h)A(h)dh$$

where h_H : maximum elevation
h_L : minimum elevation

If snow appears over the average elevation of snow line ho, hL should be replaced by ho.

From the above formula, the latitudinal distribution of snow water equivalent S(h) and the hydrometric curve A(h) should be determined in order to estimate the snow water equivalent.

It is known that the snow water equivalent increases linearly proportional to the elevation, which can ve obtained from the existing snow survey. On the other hand the catchment area can be expressed in lower order of polynomials as a function of elevation. Therefore the snow water equivalent can be estimated as a function of percentage of snow cover area in a river basin.

Figure 12.6.2 shows an estimated curve of snow water equivalent which was obtained from sample data in the three years of 1979, 1982 and 1983 in the Takaragawa River Basin, Japan. From the curve, the snow water equivalent can be estimated if the snow cover area is detected from remote sensing imagery.

Recently microwave remote sensing has been applied to estimate snow volume. Passive microwave radiometers can provide snow surface temperature with respect to inductivity of the snow, which may provide snow information. Active microwave radar can provide reflectivity or scattering of snow with respect to snow density, snow temperature, snow temperature, size of snow particles etc. It is still difficult to estimate snow volume from microwave data but several research projects are currently being carried out on this topic.

Altitudinal distribution of snow water equivalent

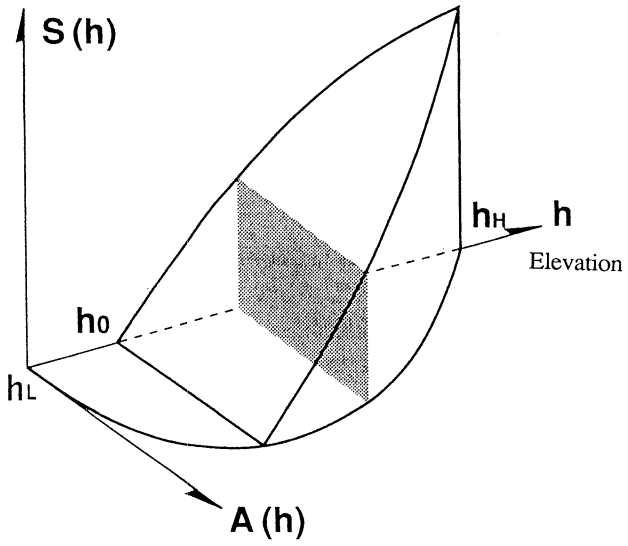

Figure 12.6.1 Estimation of basin-wide snow water equivalent

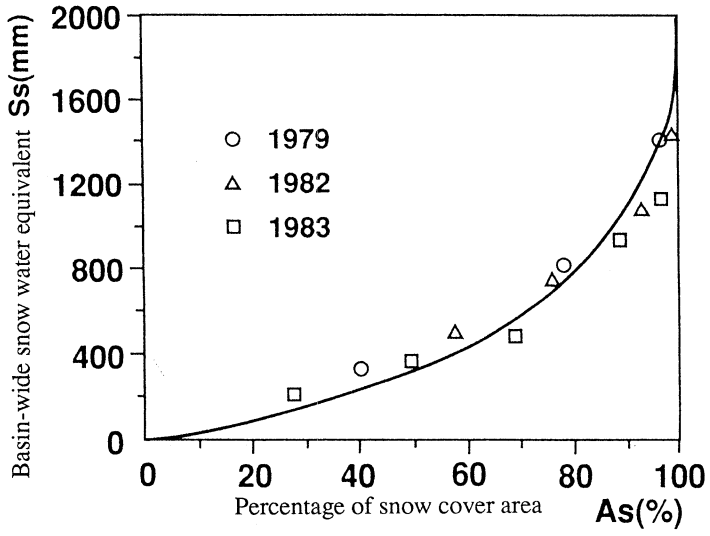

Figure 12.6.2 Result of model application to Takaragawa main stream basin

12.7 Monitoring of Atmospheric Constituents

Each **atmospheric** constituent such as water vapor, carbon-dioxidide, ozone, methane etc. has its own unique spectral characteristic of emission and absorption. With the use of these characteristics, the density of these atmospheric molecules can be monitored by measuring the spectral energy which transmits from the sun, the moon or the stars through the atmosphere, the scattering energy from the atmosphere or the clouds, the reflected energy from the earth surface and/or the thermal radiation emitted from the atmosphere and the earth surface. The spectral energy can be measured by two methods; **absorption spectroscopy** and **emission spectroscopy**.

These methods have been applied for many years ago for the measurement of the upper atmosphere from the ground. Recently the methods have been extended for measurements from aircraft, balloon and satellite. In addition, multi-spectral laser with variable wavelength, called laser rader or **lidar,** has been developed for the measurement of the spatial distribution of the atmospheric constituents.

Figure 12.7.1 shows the spectral transmittance of H2O, CO2, O3, N2O and CH4 in the infrared region.

Figure 12.7.2 shows the spectral attenuation of water vapor(H2O), and oxygen with a number of channels of the AMSU (Advanced Microwave Sounding Unit) instrument.

There are three methods used to measure the vertical distribution of atmospheric constituents; the **occultation** method which measures the attenuating light of the sun light at the sun rise and the sun sets, from a satellite, the **limb scan** method which measures the spectrum of atmosphere around the limb of the earth and the vertical viewing method, which measures the atmospheric emission from various altitudes and contribution ratio are analyzed with respect to the spectral absorption coefficient by the **inversion** method. The vertical look down method is operationally applied for carbon-dioxidide and water vapor in the infrared region and for ozone in the ultra-violet region.

Figure 12.7.3 shows the normalized **contribution function** at various wavelengths in the ultra-violet region where the vertical distribution of ozone is measured from the back scattering of blue ultra-violet (BUV) radiation.

Figure 12.7.4 shows the distribution of the integrated ozone which was measured with the TOMS (Total Ozone Mapping Spectrometer) on board Nimbus 7.

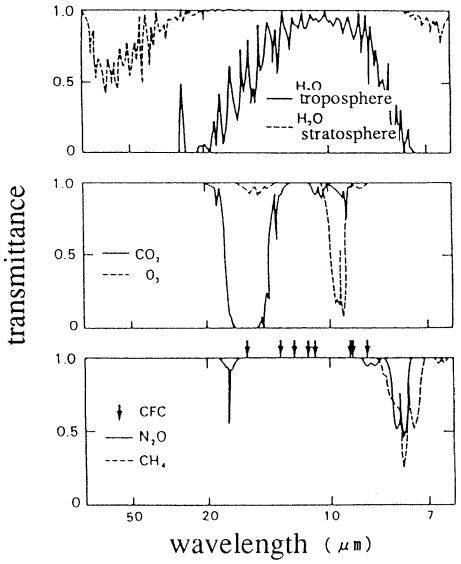

Figure 12.7.1 Spectral profile of the atmospheric transmission for thermal infrared radiation.

Indicated are the amount integrated from the ground surface to the upper end of the atmosphere. Main absorption bands of trace gases are indicated.

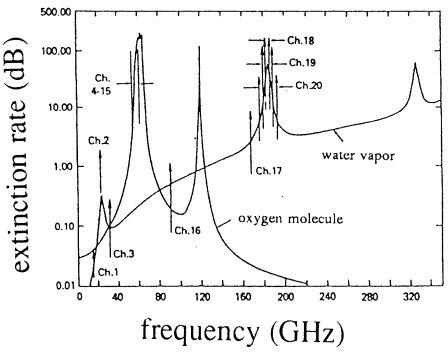

Figure 12.7.2 Atmospheric absorption spectrum in the microwave range.

Integrated vertical extinction are shown in cases of water vapor and oxygen. Channel numbers correspond to the monitoring wavelengths of the AMSU sensor (see Appendix - 1)

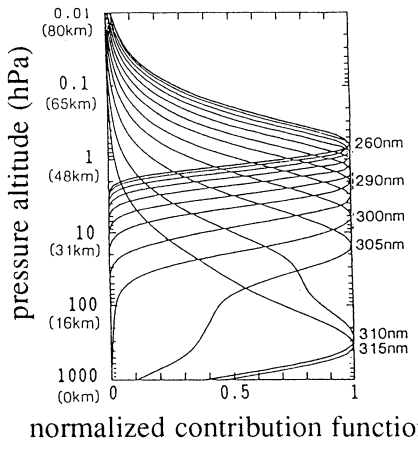

Figure 12.7.3 Vertical profile of contribution functions in each wavelength for solar ultraviolet back scattering light.

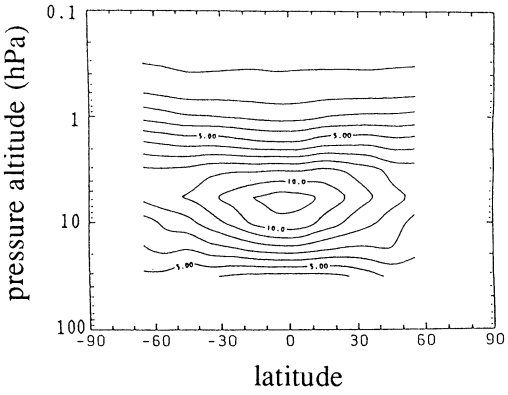

Figure 12.7.4 Altitude and latitude distribution of ozone concentration measured by the EXOS-C satellite.

The vertical axis shows the altitude in unit of pressure. The value shows the monthly average amount of volume mixing ratio (ppm) averaged in longitudinal direction in March, 1985.

12.8 Lineament Extraction

Lineament is defined as a line feature or pattern interpreted on a remote sensing image. The lineament reflects the geological structure such as faults or fractures. In this sense, the lineament extraction is very important for the application of remote sensing to geology. However the real meaning of lineament is still unclear. It should be discriminated from other line features that are not due to geological structures. Therefore the lineament extraction should be carefully interpreted by geologists.

Computer generated lineament would involve all linear features of natural terrain as well as artificial structures which have to be removed by interpretation.

Figure 12.8.1 shows an example of computer generated lineaments in the Southern Brazil region.

As lineaments can be interpreted very well on satellite images, geological survey methods have been advanced, particularly over large areas.

Lineament extraction is useful for geological analysis in oil exploration in which oil flow along faults, oil storage within faults and the oil layer can be estimated.

Lineament information can even allow analysis of the geological structure and history.

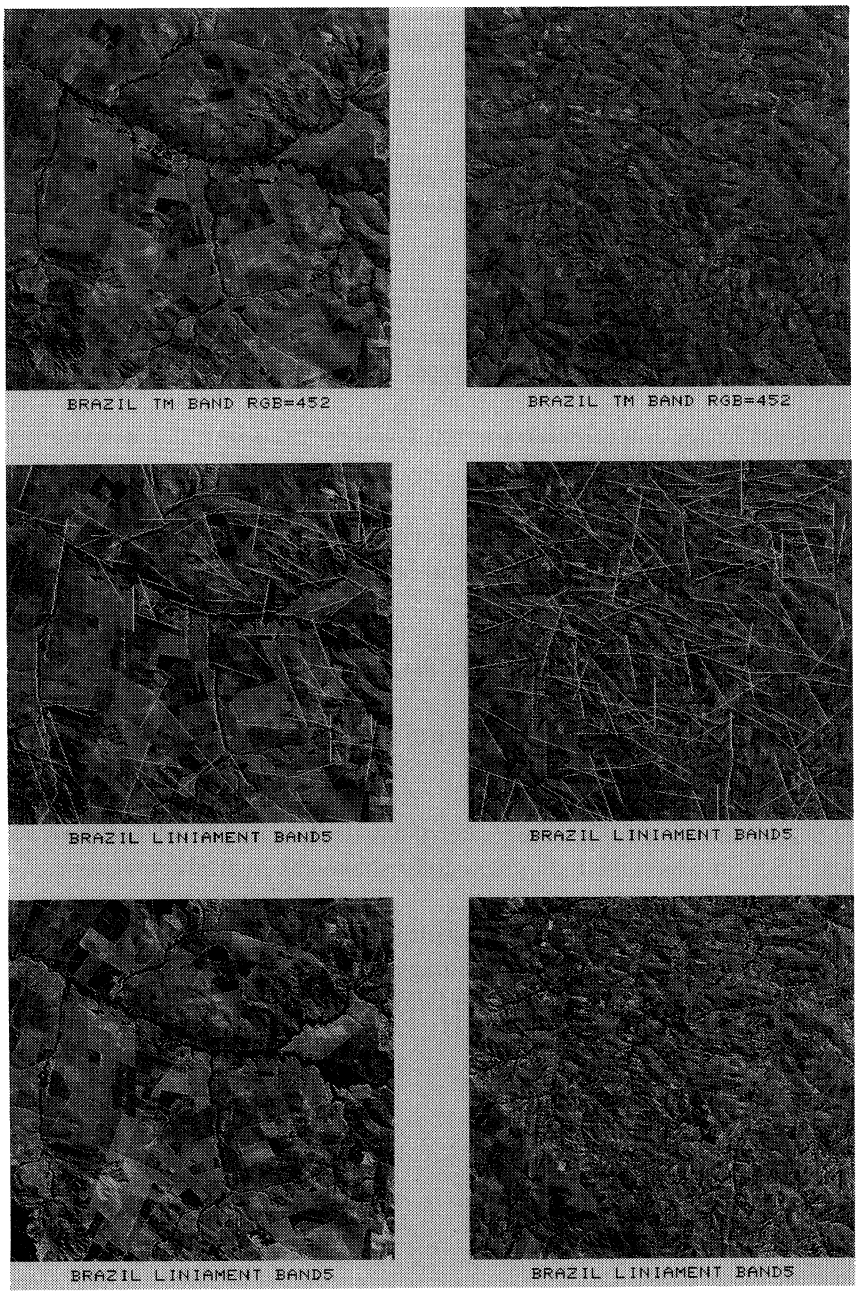

Figure 12.8.1 Semi-automatic linearment extraction by Landsat TM data

(see frontispiece 9)

12.9 Geological Interpretation

The applicability of remote sensing data increases according to the improvement in the spatial resolution as well as the spectral resolution , for example as from Landsat MSS to Landsat TM and SPOT HRV.

The advantage of satellite remote sensing in its application to geology is the wide coverage over the area of interest, where much useful information such as structural patterns and spectral features can be extracted from the imagery.

There are two ways of information extraction; geometric feature extraction with the use of geomorphologic patterns and radiometric feature extraction using the unique characteristics of spectral absorption corresponding to the rock type.

Generally visual image interpretation is most widely used in order to extract geological information from remote sensing images.

A comprehensive analysis can be carried out with geomorphologic information such as land form and slope, drainage pattern and density, and land cover.

Figure 12.9.1 (a) shows a Landsat TM image of the oil deposit basin in California, USA. Figure 12.9.1(b) shows the tectonic analysis of the same basin.

Radiometric interpretation of multi-spectral features is mainly applied to rock type classification.

Figure 12.9.2(a) shows a color composite of bands 4, 5 and 7, of Landsat TM in Gold Field, Nevada, USA, in which the light green color shows the hydrothermal zones.

Because each rock has its own spectral absorption band in the region of the short wave infrared, data from multi-spectral scanners or imaging spectrometers with multi channels is very useful for rock type classification. Thus the OPS data of JERS-1 will be useful in geology because of the shortwave infrared bands.

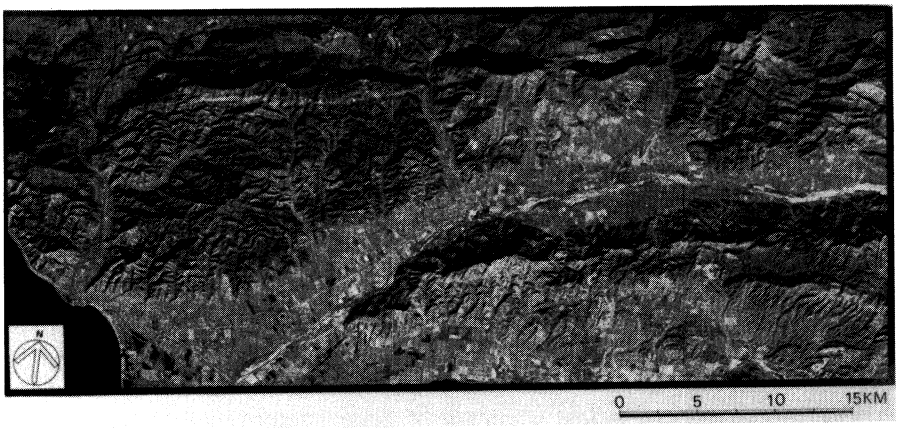

Figure 12.9.1 Color composite image of Landsat TM band 2, 3, 4 for geological analysis (Ventura basin, California)

(see frontispiece 10)

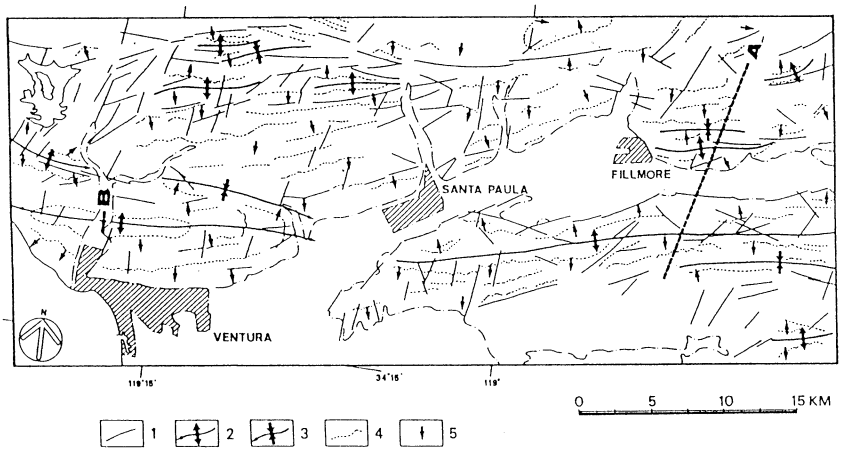

Figure 12.9.2 Tectonic analysis

1: lenearment 2: antiform 3: synform 4: bedding trace 5: dip slope

12.10 Height Measurement (DEM Generation)

Topographic mapping or **DEM** (digital elevation model) generation is possible with a pair of stereo images.

The height accuracy Δh depends on the parameters of base-height ratio (B/H) and the accuracy of parallax which may be approximated by ground resolution ΔG, as indicated as follows.

$$\Delta h = H/B \, \Delta G$$

Table 12.10.1 shows the theoretical accuracy of height determination for Landsat MSS, Landsat TM and SPOT HRV (panchromatic). In the case of SPOT HRV, with maximum base length and a B/H ratio of about 1, the height accuracy will be about 10 m the same as the ground resolution, which will be suffcient to produce topographic maps with contour lines of 40 meters interval.

There are two methods of topographic mapping or DEM generation; using operator based analytical plotters with special software, and automated DEM generation by **stereo matching**.

Usually rectified images for a pair of stereo images are initially pre-processed using ground control points.

Then stereo matching is applied to determine the conjugate points, which give x-parallax or difference of height to be converted to the height or elevation.

Figure 12.10.1 shows a pair of stereo images of SPOT HRV panchromatic data. Figure 12.10.2 shows a three dimensional view with the use of a DEM generated by stereo matching.

Table 12.10.1 Height accuracy of elevation data derived form satellite stereo images

parameter / Satellite	Satellite height	Orbital interval	Ground resolution	Height accuracy
Landsat MSS	705,000 (m)	145,000 (m)	83 (m)	400 (m)
Landsat TM	705,000 (m)	145,000 (m)	30 (m)	145 (m)
SPOT pan.	830,000 (m)	840,000 (m)	10 (m)	10 (m)

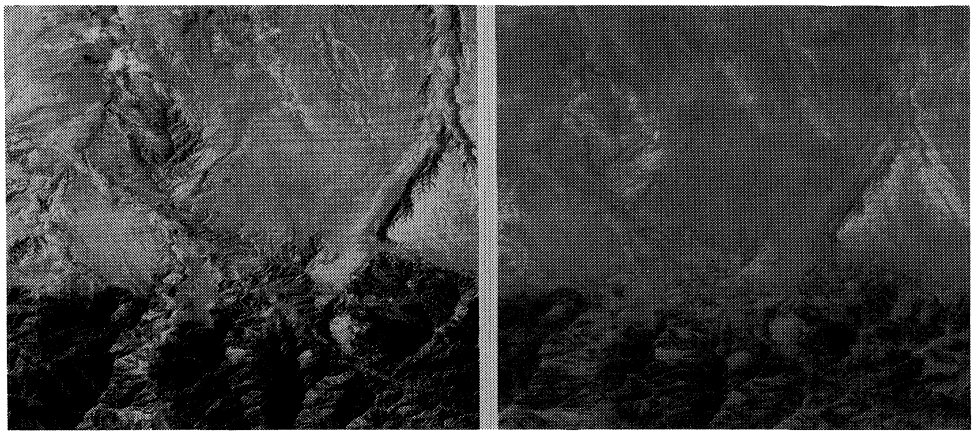

(a) Left image (b) Right image

Figure 12.10.1 SPOT stereo image

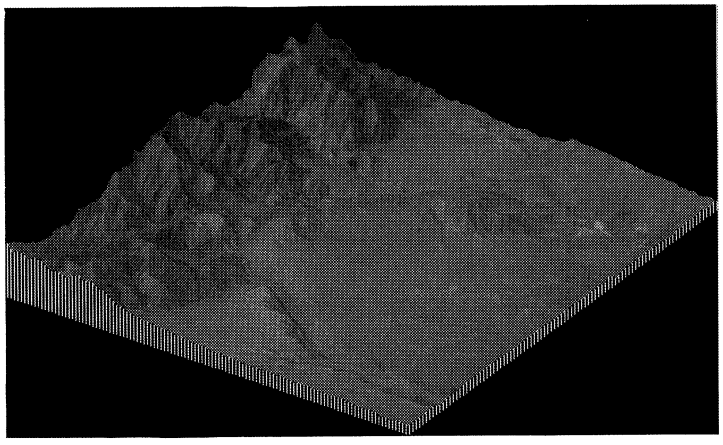

Figure 12.10.2 Bird's eye view image from north east